Ligand-Sensitized Near-Infrared to Visible Linear Light Upconversion in a Discrete Molecular Erbium Complex.

_____

Bahman Golesorkhi,[*] Soroush Naseri, Laure Guénée, Inès Taarit, Filipe Alves, Homayoun Nozary, and Claude Piguet[*]

## Supporting Information

(26 pages)

Table of contents

Experimental Section

Solvents and starting materials

Solvents and starting materials were purchased from Strem, Acros, Fluka AG and Sigma-Aldrich and used without further purification unless otherwise stated. [IR-780]I was purchased from Sigma-Aldrich. The hexafluoroacetylacetonate salts [Ln(hfa)$_3$dig] (Ln = Er, Y and Gd) were prepared from the corresponding oxides (Sigma-Aldrich, 99.99%).[S1] Ethanol, acetone, acetonitrile and dichloromethane were distilled over calcium hydride.
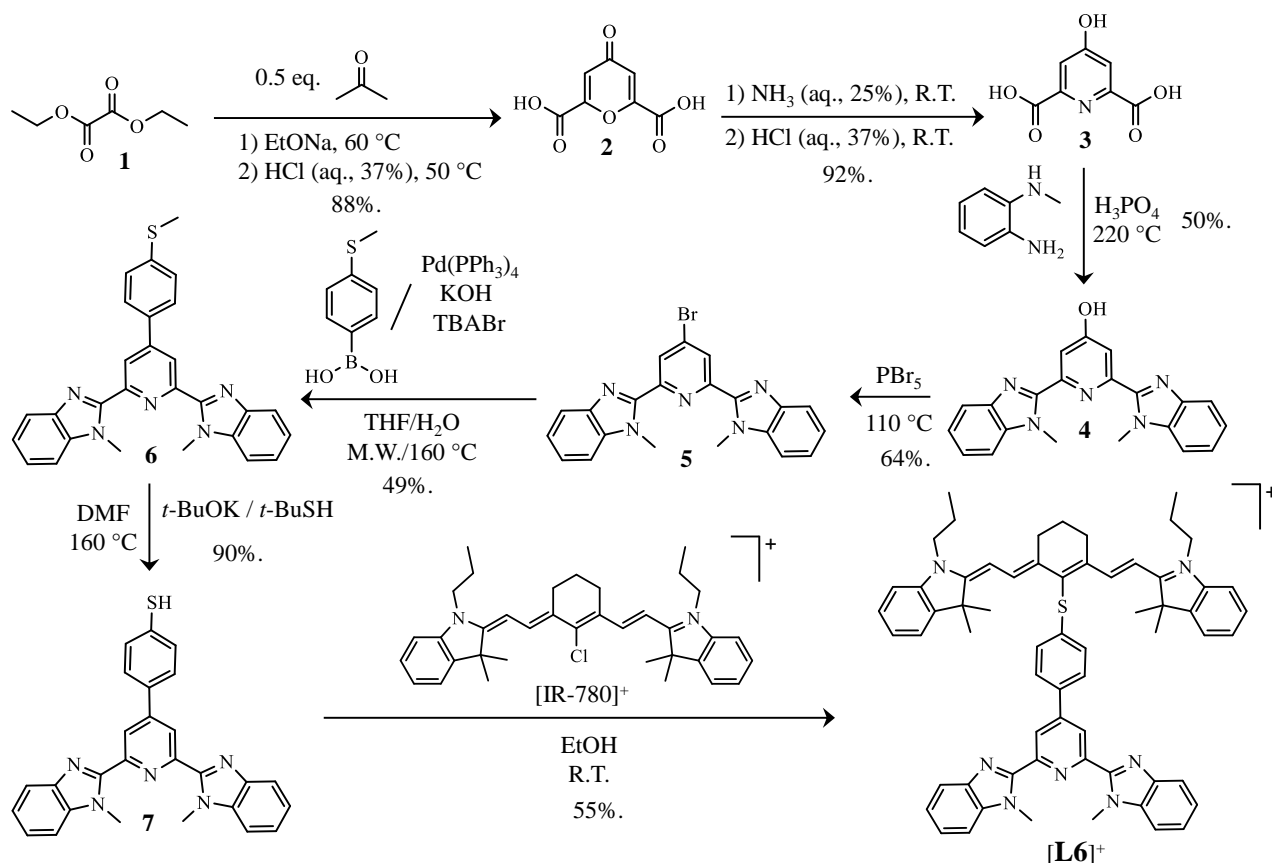
Scheme S1. Synthesis of ligand [**L6**]$^+$.

Preparation of 4-oxo-1,4-pyran-2,6-dicarboxylic acid (chelidonic acid, 2). Sodium (23.5 g, 1.02 mol, 2.04 eq.) was dissolved in dry ethanol (360 mL). A mixture of dry acetone (29.0 g, 38 mL, 0.5 mol, 1 eq.) and diethyl oxalate (**1**, 155.0 g, 144 mL, 1.06 mol, 2.12 eq.) were added to the previous solution during 15 min. A yellow precipitate was formed. The reaction mixture was kept at 60 °C for one hour. Then, HCl (aq. 37%, 200 mL) and water (100 mL) were added, and the solution was stirred at 50 °C for one day. A mixture of water and ethanol ($\approx$ 450 mL) was removed under reduced pressure. A mixture of water (300 mL) and HCl (aq. 37%, 50 mL) were then added to this mixture and stirred until a silica gel TLC (eluent: 3/7 (v/v) 10% aqueous NaCl/ethanol) showed only one spot for **2** (about three days). After cooling down to room temperature, the crystals were filtered off, washed first with

water then with cold acetone. The crude product was recrystallized from boiling water (2.5 L) using charcoal to give **2** (81.0 g, yield: 88%) as a white microcrystals. ^{1}H NMR (D$_2$O, 400 MHz), δ/ppm: 7.04 (s, 2H). ESI-MS (DMSO) *m/z:* 185.1 ([M+H]$^+$).

Preparation of 4-hydroxypyridine-2,6-dicarboxylic acid (chelidamic acid, 3). Chelidonic acid (**2**, 50.0 g , 248 mmol) was added dropwise to a solution of NH$_3$ (aq. 25%, 500 mL) at 0 °C. The resulting white suspension was stirred at room temperature for two days (after five hours, the suspension became orange). Excess of aqueous ammonia solution was removed under reduced pressure and the residue was boiled after adding water (500 mL) and charcoal (10 g). The solution was filtered and then cooled down to 5 °C. The cold solution was acidified with HCl (aq. 37%) to pH = 1. The white crystals were filtered off, washed three times with ice-cold water and dried under vacuum at 150 °C for 24 hours to give **3** (49.9 g, yield: 92%). Rf = 0.35 (silica gel TLC, 3/7 (v/v) 10% aqueous NaCl/ethanol). ^{1}H NMR (D$_2$O, 400 MHz), δ/ppm: 7.11 (s, 2H). ESI-MS (DMSO) *m/z:* 184.1 ([M+H]$^+$).

Preparation of 2,6-bis(1′-methyl-benzimidazol-2′-yl)-4-hydroxypyridine (4). Chelidamic acid (**3**, 7.0 g, 38.20 mmol, 1 eq.) and *N*-methyl-1,2-phenylenediamine (10.3 g, 84.30 mmol, 2.2 eq.) were added to phosphoric acid (85%, 25 mL) and stirred at 220 °C for 12 h. The dark blue mixture was cooled, poured into ice water (600 mL) and stirred until the formation of a light blue precipitate. The precipitate was filtered and suspended in K$_2$CO$_3$ solution (10%, 1 L). The mixture was stirred until all the solids became pink. The filtered solid was washed with water (2×100 mL) and then dissolved in hot methanol (1 L). The dark pink solution was neutralized dropwise with HCl (1.0 M) until it turned dark blue. Standing at 0 °C overnight provided gray crystals, which were filtered to give 2,6-bis(1′-methyl-benzimidazol-2′-yl)-4-hydroxypyridine (**2**, 7.0 g, yield: 50%). ^{1}H NMR (DMSO-d^6, 400 MHz), δ/ppm: 8.01 (s, 2H), 7.95 (d, ^3J = 8 Hz, 2H), 7.91 (d, ^3J = 8 Hz, 2H), 7.54 (m, 4H), 4.32 (s, 6H). ESI-MS (CHCl$_3$) *m/z:* 356 ([M+H]$^+$).

Preparation of 2,6-bis(1′-methyl-benzimidazol-2′-yl)-4-bromopyridine (5). 2,6-bis(1′-methyl-benzimidazol-2′-yl)-4-hydroxypyridine (**4**, 1.6 g, 4.50 mmol, 1eq.) was added to a flask attached with a reflux condenser. Phosphorous pentabromide (5.8 g, 13.50 mmol, 3eq.) was added to the flask and the reaction was heated at 110 °C for 16 hours under an inert atmosphere. After cooling down to room temperature, the water (50 mL) was added slowly and the pH was adjusted to 8.0 by the dropwise addition of aqueous NaOH (10%). Dichloromethane (50 mL) was added. The organic phase was separated and the aqueous layer was extracted with dichloromethane (3×50 mL). The combined organic phases were washed with brine and dried over anhydrous Na$_2$SO$_4$, filtered, and evaporated to dryness. The crude product was purified by column chromatography (Silicagel; CH$_2$Cl$_2$/methanol, 99:1) to give 2,6-bis(1′-methyl-benzimidazol-2′-yl)-4-bromopyridine (**5**, 1.2 g, yield: 64%) as a pale

yellow powder. ^{1}H NMR (CDCl$_3$, 400 MHz,), δ/ppm: 8.69 (2H, s), 7.91 (d, ^3J = 8 Hz, 2H), 7.51 (d, ^3J = 8 Hz, 2H), 7.46-7.38 (4H, m), 4.28(6H, s). ESI-MS (CHCl$_3$) *m/z:* 419 ([M+H]$^+$).

Preparation of 2,6-bis(1′-methyl-benzimidazol-2′-yl)-4-(4-(methylthio)phenyl)pyridine (6). 2,6-bis(1′-methyl-benzimidazol-2′-yl)-4-bromopyridine (**3**, 1.05 g, 2.50 mmol, 1eq.), 4-(methylthio)phenylboronic acid (0.42 g, 2.50 mmol, 1 eq.), KOH (0.70 g, 12.5 mmol, 5 eq.) , TBABr (39 mg, 0.30 mmol, 0.12 eq.) and tetrakis(triphenylphosphine)palladium (173 mg, 0.15 mmol, 0.06 eq.) together with THF (12 mL) and water (3 mL) were put in the reaction vessel. The reaction mixture was purged with argon for 15 minutes before heating it up by microwave to 160 °C for 1.5 h. After cooling down to room temperature, THF was removed under reduced pressure and water was added (30 mL). Dichloromethane (50 mL) was added and the organic phase was separated and the aqueous layer was extracted with dichloromethane (3×50 mL). The combined organic phases were washed with brine and dried over anhydrous Na$_2$SO$_4$, filtered, and evaporated to dryness. The crude product was suspended in cold ethanol and the residual solid was separated by filtration to give 2,6-bis(1′-methyl-benzimidazol-2′-yl)-4-(4-(methylthio)phenyl)pyridine (**6**, 570 mg, yield: 49%) as a pale yellow powder. ^{1}H NMR (CDCl$_3$, 400 MHz,), δ/ppm: 8.69 (2H, s), 7.93 (d, ^3J = 8 Hz, 2H), 7.89 (d, ^3J = 8 Hz, 2H), 7.51 (d, ^3J = 8 Hz, 2H), 7.45-7.38 (6H, m), 4.30 (6H, s), 2.57 (3H, s). ^{13}C NMR (CD$_2$Cl$_2$, 100 MHz,), δ/ppm: aliphatic CH$_2$+CH$_3$: 15.06, 32.61; aromatic C + CH: 110.05, 119.89, 122.29, 122.59, 123.41, 126.33, 127.50, 133.44, 137.43, 141.30, 142.69, 149.52, 150.37, 150.47. ESI-MS (CHCl$_3$) *m/z:* 462 ([M+H]$^+$).

Preparation of 2,6-bis(1′-methyl-benzimidazol-2′-yl)-4-(4-(mercapto)phenyl)pyridine (7). 2,6-bis(1′-methyl-benzimidazol-2′-yl)-4-(4-(methylthio)phenyl)pyridine (**6**, 600 mg, 1.3 mmol, 1eq.) and potassium *tert*-butoxide (1.16 g, 10.4 mmol, 8 eq.) were dissolved in dry DMF (15 mL) under exclusion of air and water. *Tert*-butylthiol (586 mg, 6.5 mmol, 5 eq.) was injected to the mixture and the reaction mixture was heated at 160 °C under reflux and inert atmosphere for 15 h. After cooling down to 5-8 °C, the reaction mixture was poured into a quasi-saturated aqueous ammonium chloride solution (100 mL, pH ≈ 5) and a pale yellow solid was precipitated. The product was then collected on a fritted glass after a filtration, and washed several times with cold water to give 2,6-bis(1′-methyl-benzimidazol-2′-yl)-4-(4-(mercapto)phenyl)pyridine (**7**, 526 mg, yield: 90%) as a pale yellow powder. ^{1}H NMR (CDCl$_3$, 400 MHz,), δ/ppm: 8.70 (2H, s), 7.91 (d, ^3J = 8 Hz, 2H), 7.84 (d, ^3J = 8 Hz, 2H), 7.53 (d, ^3J = 8 Hz, 2H), 7.44-7.34 (6H, m), 4.30(6H, s). ^{13}C NMR (CD$_2$Cl$_2$, 100 MHz,), δ/ppm: aliphatic CH$_2$+CH$_3$: 33.24; aromatic C + CH: 111.76, 119.43, 122.51, 122.80, 123.60, 124.20, 124.25, 128.13, 128.74, 132.90, 137.19, 149.10, 149.20, 149.50. ESI-MS (CHCl$_3$) *m/z:* 448 ([M+H]$^+$).

Preparation of [L6](PF₆). 2,6-bis(1′-methyl-benzimidazol-2′-yl)-4-(4-(mercapto)phenyl)pyridine (**7**, 604 mg, 1.35 mmol, 1.05 eq.) and [IR-780]I (855 mg, 1.28 mmol, 1.0 eq.) were dissolved in dry ethanol (50 mL) and the reaction mixture was stirred at room temperature for 48 h under N_2. The solvent was evaporated to dryness and the solid residual was dissolved in dichloromethane (30 mL). Saturated aqueous solution of potassium hexafluorophosphate (10 mL) was added and the mixture was gently shacked. The organic phase was separated and the aqueous layer was extracted with dichloromethane (3×20 mL). The combined organic phases were washed several times with water, dried over anhydrous Na_2SO_4, filtered, and evaporated to dryness. The crude product was purified by crystallization induced by slow diffusion of diethyl ether into a saturated dichloromethane solution of the product to give [**L6**](PF₆)·0.75CH₂Cl₂·0.1H₂O·C₄H₁₀O (772 mg, yield: 55%, calcd C 65.89, H 5.82, N 8.31; found C 65.96, H 5.74, N 8,20) as dark red crystals suitable for X-ray diffraction studies. ¹H NMR (CD₂Cl₂, 400 MHz,), δ/ppm: 8.815 (d, ^3J = 12 Hz, 2H), 8.64 (s, 2H), 7.875 (d, ^3J = 12 Hz, 2H), 7.80 (d, ^3J = 8 Hz, 2H), 7.54 (d, ^3J = 8 Hz, 2H), 7.47-7.34 (m, 10H), 7.27(t, ^3J = 8 Hz, 2H), 7.15 (d, ^3J = 8 Hz, 2H), 6.205 (d, ^3J = 12 Hz, 2H), 4.30 (s, 6H), 4.02 (t, ^3J = 8 Hz, 4H), 2.81 (t, ^3J = 8 Hz, 4H), 2.11 (qui, ^3J = 4 Hz, 2H), 1.92 (sextet, ^3J = 8 Hz, 4H), 1.55 (s, 12H), 1.09 (t, ^3J = 8 Hz, 6H). ¹³C NMR (CD₂Cl₂, 100 MHz,), δ/ppm: aliphatic CH₂+CH₃: 11.74, 21.22, 21.29, 26.79, 28.15, 30.10, 33.03, 46.39, 49.79; aromatic C + CH: 101.60, 110.56, 11.12, 120.16, 122.68, 122.72, 123.11, 123.98, 125.75, 127.13, 128.63, 129.04, 133.92, 135.05, 137.83, 139.95, 141.63, 142.63, 143.00, 147.79, 149.50, 150.66, 150.85, 151.49, 173.34. ESI-MS (CHCl₃) *m/z:* 950 ([M]⁺), 936 ([M-CH₃]⁺), 922 ([M-(CH₃)₂]⁺).

Preparation of [L6Er(hfa)₃](PF₆). Stoichiometric amounts of [**L6**](PF₆) (300 mg, 0.159 mmol, 1.0 eq.) and [Er(hfa)₃dig]·xH₂O (147 mg, 0.159 mmol, 1.0 eq.) were dissolved and stirred in dichloromethane/acetonitrile (1:1, 20 mL). Dropwise addition of *tert*-butyl methyl ether (20 mL) yielded microcrystalline powder for which the elemental analysis was compatible with the formation of [**L6**Er(hfa)₃](PF₆)·2.0CH₃CN·1.9C₅H₁₂O complex (190 mg, yield: 63%, calcd C 51.49, H 4.52, N 5.91; found C 51.77, H 4.25, N 5.64). Slow diffusion of diethyl ether into the concentrated dichloromethane solution of the latter microcrystalline powder provided dark red crystals of [**L6**Er(hfa)₂(O₂CCF₃)](PF₆) suitable for X-ray diffraction studies.

Preparation of [L6Y(hfa)₃](PF₆). Stoichiometric amounts of [**L6**](PF₆) (0.012 mmol, 1.0 eq.) and [Y(hfa)₃dig]·xH₂O (0.012 mmol, 1.0 eq.) were dissolved and stirred in dichloromethane/acetonitrile (1:1, 5 mL). Dropwise addition of diethyl ether (5 mL) yielded microcrystalline powder which was filtered and dried over vacuum. Elemental analysis was compatible with the formation of [**L6**Y(hfa)₃](PF₆)·1.84CH₂Cl₂·0.9C₄H₁₀O complex calcd C 49.36, H 3.94, N 4.84; found C 49.64, H 3.66, N 4.56.

Preparation of [L6Gd(hfa)₃](PF₆). Stoichiometric amounts of [**L6**](PF$_6$) (0.012 mmol, 1.0 eq.) and [Gd(hfa)$_3$dig]·xH$_2$O (0.012 mmol, 1.0 eq.) were dissolved and stirred in dichloromethane/acetonitrile (1:1, 5 mL). Evaporation to dryness followed by re-dissolution in CH$_3$CN (24 mL) gave a final solution at $|\mathbf{L6}|_{\text{tot}} = |\text{Gd}|_{\text{tot}} = 5 \cdot 10^{-4}$ M which was used for photophysical measurements.

Spectroscopic and analytical measurements

^{1}H NMR spectra were recorded at 293 K on a Bruker Avance 400 MHz spectrometer. Chemical shifts are given in ppm with respect to tetramethylsilane Si(CH$_3$)$_4$ (TMS). Spectral assignment was assisted by 2D COSY NMR experiment where appropriate. Pneumatically-assisted electrospray (ESI) mass spectra were recorded from 10^{-4} M solutions on an API 150EX (AB/MDS Sciex) equipped with a Turbo Ionspray source®. Elemental analyses were performed by K. L. Buchwalder from the Microchemical Laboratory of the University of Geneva.

Solid-state luminescence data were collected on samples mounted directly onto copper plates using conductive silver glue. Emission spectra were measured on a Horiba Scientific Fluorolog 3 spectrofluorimeter equipped with a visible photomultiplier tube (PMT) (220-850 nm, R928P, Hamamatsu). The infrared luminescence spectra were recorded using a NIR-PMT cooled to -80 °C (300-1700 nm, R5509-73, Hamamatsu) and a 850 nm longpass filter (Thorlabs) upon 801 nm laser excitation. The standard xenon lamp of the Horiba Scientific Fluorolog 3 spectrofluorimeter has been used for UV excitation of the samples to record the pertinent emission spectra, where the appropriate longpass filters (Thorlabs) have been placed after the sample to remove the second-order Rayleigh scattering of the xenon lamp. The low-temperature emission spectra were recorded using an optical closed-cycle cryostat capable of reaching low temperatures down to 5 K in a helium atmosphere (Sumitono HC-4E/Janis Research CCS-900/204N), For the low-temperature solution measurements inside the cryostat, the solution sample was placed in a quartz capillary which was then stuck onto a copper plate using optically transparent silver glue. The emission spectra were corrected for the instrumental response function. Continuous NIR laser excitation was achieved with a diode laser MLL-H-800-2.5W (801 nm) from Changchun New Industries Optoelectronics Technology Co., Ltd (CNI). A 550/88 nm bandpass filter (Semrock) was placed directly after the sample for visible emission measurements in order to remove the second-order Rayleigh scattering of the laser line. The excitation beam was loosely focused onto the sample with a 30 cm lens to reach an excitation spot size of ≈1.5 mm in diameter (Surface ≈ 0.07 cm^2). The mathematical analyses were performed by using Igor Pro® (WaveMetrics Inc.), Origin 2017 (OriginLab Corporation) and Excel® (Microsoft) software. The upconversion quantum yields were determined through the relative method using indocyanine green as the reference (ICG, $\lambda_{\text{exc}} = 801$ nm, $\Phi^{\text{ref}} = 0.132$ in ethanol at 293 K, $n_{\text{acetonitrile}} = 1.344$).[S2] Quantitative data for the upconversion process were obtained by using indocyanine green

(ref) and eq. S1, where Φ is the quantum yield, E is the integrated emission spectrum, A is the absorbance at the excitation wavelength λ, n is the refractive index ($n_{\text{acetonitrile}} = 1.344$ and $n_{\text{ethanol}} = 1.361$), P_{exc} is the power intensity of the excitation source at the excitation wavelength and $h\nu_{\text{exc}}$ is the energy of the incident photon at frequency $\nu_{\text{exc}} = (c/\lambda_{\text{exc}})$ so that $I_{\text{exc}} = P_{\text{exc}}/h\nu_{\text{exc}}$ is the spectral radiant power measuring the incident excitation intensity.

$$\frac{\Phi^{\text{up}}}{\Phi^{\text{ref}}} = \frac{E_{\text{up}}}{E_{\text{ref}}} \cdot \frac{A_{\text{ref}}}{A_{\text{up}}} \cdot \frac{n_{\text{ref}}^2}{n_{\text{up}}^2} \cdot \frac{P_{\text{exc,ref}}}{P_{\text{exc,up}}} \cdot \frac{h\nu_{\text{exc,up}}}{h\nu_{\text{exc,ref}}} \tag{S1}$$

Because of the considerable absorbance of the sample at a fixed complex concentration of $5 \cdot 10^{-4}$ M in acetonitrile, the geometry of the measuring cell was optimized (position and rotation) so that the laser-diode 801 nm beam went through a width compatible with the detection of transmitted light at 801 nm along the original excitation direction. The detector was then focused on the part of the solution in the cell which was excited by the excitation beam. Having fixed all these parameters, the upconversion emission spectra was recorded. The indocyanine green reference was then measured in the same conditions and extreme care were taken for having identical location of the incident beam and detector. The concentration of the reference was adapted so that its emission intensity was comparable with that of the sample using the same excitation power. Electronic absorption spectra in the Visible and NIR regions were recorded at 293 K from acetonitrile (ethanol for ICG) solutions with a Perkin-Elmer Lambda 1050 absorption spectrometer using quartz cell of 0.1, 1 and 10 mm path length. Solution emission spectra were recorded in non-deuterated acetonitrile (non-deuterated ethanol for ICG) using quartz cells of 10 mm path length. The emission spectrum of ICG was recorded upon excitation at $\lambda_{\text{exc}} = 705$ nm using the standard xenon lamp of the Horiba Scientific Fluorolog 3 spectrofluorimeter. The emission spectra were corrected for the instrumental response function.

X-ray crystallography

Summary of crystal data, intensity measurements and structure refinements for ligand [**L6**](PF$_6$) and complex [**L6**Er(hfa)$_2$(O$_2$CCF$_3$)](PF$_6$)·(CH$_3$CH$_2$)$_2$O were collected in Tables S1 and S4. Pertinent bond lengths, bond angles and interplanar angles were collected in Tables S2-S3 and S5-S6 together with ORTEP views and the pertinent numbering schemes and intermolecular interactions gathered in Figures S1-S2. The crystals were mounted on Hampton cryoloops with protection oil. X-ray data collections were performed with a XtaLAB Synergy-S diffractometer equipped with an hybrid pixel hypix arc 150 detector. The structures were solved by using dual-space algorithm SHELXT.[S3] Full-matrix least-square refinements on F^2 were performed with SHELX2015.[S3] CCDC 2091958-2091959 contain the supplementary crystallographic data. These data can be obtained free of charge from the Cambridge Crystallographic Data Centre via www.ccdc.cam.ac.uk/.

Shape Analysis

The geometry of the [**L6**Er(hfa)$_2$(O$_2$CCF$_3$)]$^+$ unit was analyzed with the program Shape 2.1.[S4]

Polyhedron	Point group	Shape's score
Enneagon	D_{9h}	33.447
Octagonal pyramid	C_{8v}	23.084
Heptagonal bipyramid	D_{7h}	19.176
Johnson triangular cupola	C_{3v}	13.976
Capped cube	C_{4v}	9.131
Spherical-relaxed capped cube	C_{4v}	8.688
Capped square antiprism	C_{4v}	2.071
Spherical capped square antiprism	C_{4v}	1.660
Tricapped trigonal prism	D_{3h}	2.325
Spherical tricapped trigonal prism	D_{3h}	1.921
Tridiminished icosahedron	C_{3v}	12.983
Hula-hoop	C_{2v}	11.301
Muffin	C_s	1.320

Among the possible arrangements for the nine-coordinated EuN$_3$O$_6$ unit, the lowest value of deviation (score = 1.320) was found for a C_s-symmetrical distorted muffin shape. Deviation for the next closest model, i.e. a C_{4v}-symmetrical spherical capped square antiprism arrangement, amounts to 1.660.

References

S1   a) Malandrino, G.; Incontro, O.; Castelli, F.; Fragalà, I. L.; Benelli, C., Synthesis, Characterization, and Mass-Transport Properties of Two Novel Gadolinium(III) Hexafluoroacetylacetonate Polyether Adducts: Promising Precursors for MOCVD of GdF$_3$ Films. *Chem. Mater.* **1996**, *8*, 1292-1297; b) Evans, W. J.; Giarikos, D. G.; Johnston, M. A.; Greci, M. A.; Ziller, J. W., Reactivity of the Europium Hexafluoroacetylacetonate (hfac) Complex, Eu(hfac)$_3$(diglyme), and Related Analogs with Potassium: Formation of the Fluoride hfac "ate" Complexes, [LnF(hfac)$_3$K(diglyme)]$_2$. *J. Chem. Soc., Dalton Trans.* **2002**, 520-526; c) Malandrino, G.; Lo Nigro, R.; Fragalà, I. L.; Benelli, C., Yttrium β-Diketonate Glyme MOCVD Precursors: Effects of the Polyether Length on Stabilities, Mass Transport Properties and Coordination Spheres. *Eur. J. Inorg. Chem.* **2004**, 500-509.

S2   a) Rurack, K.; Spieles, M., Fluorescence Quantum Yields of a Series of Red and Near-Infrared Dyes Emitting at 600-1000 nm. *Anal. Chem.* **2011**, *83* (4), 1232-1242; b) Würth, C.; Grabolle, M.; Pauli, J.; Spieles, M.; Resch-Genger, U., Relative and Absolute Determination of

Fluorescence Quantum Yields of Transparent Samples. *Nat. Protoc.* **2013**, *8*, 1535-1550; c) Souri, N.; Tian, P.; Platas-Iglesias, C.; Wong, K.-L.; Nonat, A.; Charbonnière, L. J., Upconverted Photosensitization of Tb Visible Emission by NIR Yb Excitation in Discrete Supramolecular Heteropolynuclear Complexes. *J. Am. Chem. Soc.* **2017**, *139*, 1456-1459; d) Nonat, A.; Bahamyirou, S.; Lecointre, A.; Przybilla, F.; Mély, Y.; Platas-Iglesias, C.; Camerel, F.; Jeannin, O.; Charbonnière, L. J., Molecular Upconversion in Water in Heteropolynuclear Supramolecular Tb/Yb Assemblies. *J. Am. Chem. Soc.* **2019**, *141*, 1568-1576.

S3   Sheldrick, G. M., Crystal Structure Refinement with SHELXL. *Acta Cryst. C Structural Chemistry* **2015**, *71*, 3-8.

S4   a) SHAPE is a free software developed by Llunell, M; Casanova, D.; Cirera, J.; Alemany, P.; Alvarez, S. and available online at http://www.ee.ub.edu/; b) Pinsky, M.; Avnir, D., Continuous Symmetry Measures. 5. The Classical Polyhedral. *Inorg. Chem.* **1998**, *37*, 5575-5582; c) Casanova, D.; Cirera, J.; Llunell, M.; Alemany, P.; Avnir, D.; Alvarez, S., Minimal Distortion Pathways in Polyhedral Rearrangements. *J. Am. Chem. Soc.* **2004**, *126*, 1755-1763; d) Alvarez, S., Polyhedra in (Inorganic) Chemistry. *Dalton Trans.* **2005**, 2209-2233.

Table S1. Summary of crystal data, intensity measurements and structure refinements for ligand [**L6**](PF$_6$).

	[**L6**](PF$_6$)
Empirical formula	C$_{66.05}$H$_{71.46}$Cl$_{0.63}$F$_6$N$_7$O$_{0.68}$PS
Chemical formula moiety	C$_{63}$H$_{64}$N$_7$S, PF$_6$, 0.683(C$_4$H$_{10}$O), 0.317(CH$_2$Cl$_2$)
Formula weight	1173.79
Temperature	150.00(10) K
Wavelength	1.54184 Å
Crystal System, Space group	Monoclinic, *P* 21/*c*
Unit cell dimensions	a = 16.10494(16) Å, b = 20.80762(16) Å, c = 18.64005(16) Å, α = 90°, β = 101.9679(9)°, γ = 90°
Volume in Å^3	6110.61(10)
Z, Calculated density	4, 1.276 Mg/m^3
Absorption coefficient	1.519 mm^{-1}
F(000)	2472
Theta range for data collection	2.805 to 74.398°
Limiting indices	-19≤h≤20, -23≤k≤25, -22≤l≤23
Reflections collected / unique	166820 / 12377 [*R*(int) = 0.0374]
Completeness to theta	67.684°/ 99.9 %
Data / restraints / parameters	12377 / 0 / 764
Goodness-of-fit on *F*^{2}	1.069
Final *R* indices [*I*>2σ(*I*)]	R_1 = 0.0682, ωR_2 = 0.2028
R indices (all data)	R_1 = 0.0799, ωR_2 = 0.2127
Largest diff. peak and hole	0.974 and -0.755 e.Å^{-3}

Table S2. Selected bond distances (Å) and bond angles (°) for ligand [**L6**](PF$_6$).

Bond distances (Å)

Atom 1	Atom 2	Distance	Atom 1	Atom 2	Distance
S(1)	C(25)	1.779(2)	C(23)	C(24)	1.385(3)
S(1)	C(28)	1.793(3)	C(24)	C(25)	1.388(3)
N(1)	C(5)	1.348(3)	C(25)	C(26)	1.390(4)
N(1)	C(68)	1.339(3)	C(26)	C(27)	1.382(4)
N(2)	C(6)	1.311(3)	C(28)	C(29)	1.423(4)
N(2)	C(7)	1.389(3)	C(28)	C(33)	1.405(3)
N(3)	C(6)	1.375(3)	C(29)	C(30)	1.510(4)
N(3)	C(12)	1.392(3)	C(29)	C(49)	1.387(3)
N(3)	C(13)	1.452(4)	C(30)	C(31)	1.514(4)
N(4)	C(14)	1.325(4)	C(31)	C(32)	1.528(4)
N(4)	C(15)	1.381(4)	C(32)	C(33)	1.499(4)
N(5)	C(14)	1.377(3)	C(33)	C(34)	1.410(4)
N(5)	C(20)	1.386(4)	C(34)	C(35)	1.383(3)
N(5)	C(21)	1.459(4)	C(35)	C(36)	1.400(4)
N(6)	C(36)	1.345(3)	C(36)	C(37)	1.535(4)
N(6)	C(45)	1.414(4)	C(37)	C(38)	1.542(4)
N(6)	C(46)	1.466(4)	C(37)	C(39)	1.540(4)
N(7)	C(51)	1.366(4)	C(37)	C(40)	1.517(4)
N(7)	C(60)	1.419(4)	C(40)	C(41)	1.381(4)
N(7)	C(61)	1.458(5)	C(40)	C(45)	1.387(4)
C(2)	C(3)	1.392(4)	C(41)	C(42)	1.390(5)
C(2)	C(68)	1.401(4)	C(42)	C(43)	1.394(5)
C(3)	C(4)	1.387(4)	C(43)	C(44)	1.389(5)
C(3)	C(22)	1.479(3)	C(44)	C(45)	1.392(4)
C(4)	C(5)	1.388(4)	C(46)	C(47)	1.520(5)
C(5)	C(6)	1.480(4)	C(47)	C(48)	1.516(5)
C(7)	C(8)	1.402(4)	C(49)	C(50)	1.406(4)
C(7)	C(12)	1.395(4)	C(50)	C(51)	1.379(4)
C(8)	C(9)	1.376(4)	C(51)	C(52)	1.527(4)
C(9)	C(10)	1.405(5)	C(52)	C(53)	1.532(4)
C(10)	C(11)	1.384(4)	C(52)	C(54)	1.532(4)
C(11)	C(12)	1.381(4)	C(52)	C(55)	1.507(4)
C(14)	C(68)	1.475(4)	C(55)	C(56)	1.380(4)
C(15)	C(16)	1.397(4)	C(55)	C(60)	1.370(5)
C(15)	C(20)	1.401(4)	C(56)	C(57)	1.405(5)
C(16)	C(17)	1.374(5)	C(57)	C(58)	1.348(7)
C(17)	C(18)	1.394(6)	C(58)	C(59)	1.403(6)
C(18)	C(19)	1.385(5)	C(59)	C(60)	1.384(4)
C(19)	C(20)	1.397(4)	C(61)	C(62)	1.455(7)
C(22)	C(23)	1.388(4)	C(62)	C(63)	1.467(7)
C(22)	C(27)	1.396(3)			

Angles (°)

At. 1	At. 2	At. 3	angle	At. 1	At. 2	At. 3	angle
C(25)	S(1)	C(28)	100.3(1)	C(33)	C(28)	S(1)	118.7(2)
C(68)	N(1)	C(5)	116.9(2)	C(33)	C(28)	C(29)	122.7(2)
C(6)	N(2)	C(7)	104.6(2)	C(28)	C(29)	C(30)	118.9(2)
C(6)	N(3)	C(12)	105.8(2)	C(49)	C(29)	C(28)	120.6(2)
C(6)	N(3)	C(13)	128.8(2)	C(49)	C(29)	C(30)	120.5(2)
C(12)	N(3)	C(13)	125.3(2)	C(29)	C(30)	C(31)	112.9(2)
C(14)	N(4)	C(15)	105.4(2)	C(30)	C(31)	C(32)	110.0(3)
C(14)	N(5)	C(20)	106.1(2)	C(33)	C(32)	C(31)	109.7(2)
C(14)	N(5)	C(21)	130.5(2)	C(28)	C(33)	C(32)	117.3(2)
C(20)	N(5)	C(21)	123.4(2)	C(28)	C(33)	C(34)	120.2(2)
C(36)	N(6)	C(45)	111.6(2)	C(34)	C(33)	C(32)	122.4(2)
C(36)	N(6)	C(46)	125.7(2)	C(35)	C(34)	C(33)	127.3(3)
C(45)	N(6)	C(46)	122.6(2)	C(34)	C(35)	C(36)	122.4(3)
C(51)	N(7)	C(60)	110.7(3)	N(6)	C(36)	C(35)	122.8(3)
C(51)	N(7)	C(61)	125.0(3)	N(6)	C(36)	C(37)	109.0(2)
C(60)	N(7)	C(61)	123.8(3)	C(35)	C(36)	C(37)	128.3(2)
C(3)	C(2)	C(68)	119.2(2)	C(36)	C(37)	C(38)	111.4(2)
C(2)	C(3)	C(22)	120.9(2)	C(36)	C(37)	C(39)	113.1(2)
C(4)	C(3)	C(2)	117.9(2)	C(39)	C(37)	C(38)	111.2(2)
C(4)	C(3)	C(22)	121.2(2)	C(40)	C(37)	C(36)	101.2(2)
C(3)	C(4)	C(5)	119.1(2)	C(40)	C(37)	C(38)	109.2(2)
N(1)	C(5)	C(4)	123.8(2)	C(40)	C(37)	C(39)	110.2(2)
N(1)	C(5)	C(6)	117.9(2)	C(41)	C(40)	C(37)	130.9(3)
C(4)	C(5)	C(6)	118.4(2)	C(41)	C(40)	C(45)	119.8(3)
N(2)	C(6)	N(3)	113.8(2)	C(45)	C(40)	C(37)	109.2(3)
N(2)	C(6)	C(5)	122.2(2)	C(40)	C(41)	C(42)	118.9(3)
N(3)	C(6)	C(5)	124.0(2)	C(41)	C(42)	C(43)	120.5(3)
N(2)	C(7)	C(8)	129.6(3)	C(44)	C(43)	C(42)	121.4(3)
N(2)	C(7)	C(12)	110.5(2)	C(43)	C(44)	C(45)	116.7(3)
C(12)	C(7)	C(8)	119.9(3)	C(40)	C(45)	N(6)	108.9(2)
C(9)	C(8)	C(7)	117.9(3)	C(40)	C(45)	C(44)	122.6(3)
C(8)	C(9)	C(10)	121.2(3)	C(44)	C(45)	N(6)	128.5(3)
C(11)	C(10)	C(9)	121.5(3)	N(6)	C(46)	C(47)	112.2(2)
C(12)	C(11)	C(10)	116.9(3)	C(48)	C(47)	C(46)	111.7(3)
N(3)	C(12)	C(7)	105.3(2)	C(29)	C(49)	C(50)	126.6(3)
C(11)	C(12)	N(3)	132.0(3)	C(51)	C(50)	C(49)	123.6(3)
C(11)	C(12)	C(7)	122.6(3)	N(7)	C(51)	C(50)	123.2(3)
N(4)	C(14)	N(5)	112.8(2)	N(7)	C(51)	C(52)	108.3(2)
N(4)	C(14)	C(68)	121.0(2)	C(50)	C(51)	C(52)	128.4(3)
N(5)	C(14)	C(68)	126.2(2)	C(51)	C(52)	C(53)	111.9(2)
N(4)	C(15)	C(16)	130.1(3)	C(51)	C(52)	C(54)	112.1(2)
N(4)	C(15)	C(20)	109.8(3)	C(53)	C(52)	C(54)	111.4(3)
C(16)	C(15)	C(20)	120.0(3)	C(55)	C(52)	C(51)	101.9(2)
C(17)	C(16)	C(15)	118.1(4)	C(55)	C(52)	C(53)	110.2(2)
C(16)	C(17)	C(18)	121.3(3)	C(55)	C(52)	C(54)	108.9(2)
C(19)	C(18)	C(17)	122.2(3)	C(56)	C(55)	C(52)	130.0(3)
C(18)	C(19)	C(20)	116.2(3)	C(60)	C(55)	C(52)	109.6(3)
N(5)	C(20)	C(15)	105.9(2)	C(60)	C(55)	C(56)	120.3(3)
N(5)	C(20)	C(19)	131.9(3)	C(55)	C(56)	C(57)	117.6(4)

Angles (°)

At. 1	At. 2	At. 3	angle	At. 1	At. 2	At. 3	angle
C(19)	C(20)	C(15)	122.2(3)	C(58)	C(57)	C(56)	121.2(4)
C(23)	C(22)	C(3)	121.0(2)	C(57)	C(58)	C(59)	121.9(3)
C(23)	C(22)	C(27)	118.3(2)	C(60)	C(59)	C(58)	116.0(4)
C(27)	C(22)	C(3)	120.7(2)	C(55)	C(60)	N(7)	109.3(3)
C(24)	C(23)	C(22)	121.0(2)	C(55)	C(60)	C(59)	122.9(3)
C(23)	C(24)	C(25)	120.1(2)	C(59)	C(60)	N(7)	127.8(4)
C(24)	C(25)	S(1)	119.03(19)	C(62)	C(61)	N(7)	112.7(4)
C(24)	C(25)	C(26)	119.6(2)	C(61)	C(62)	C(63)	114.9(5)
C(26)	C(25)	S(1)	121.36(18)	N(1)	C(68)	C(2)	123.0(2)
C(27)	C(26)	C(25)	119.9(2)	N(1)	C(68)	C(14)	119.7(2)
C(26)	C(27)	C(22)	121.0(2)	C(2)	C(68)	C(14)	117.3(2)
C(29)	C(28)	S(1)	118.51(18)				

Table S3. Selected least-squares planes data for ligand [**L6**](PF$_6$).

Least-squares planes

Least-squares planes description	Abbreviation	Max. dev./Å	Atom
Benzimidazole 1	Bz1	0.018	N(2),N(3),
C(7) C(8) C(9) C(10) C(11) C(12) N(3) C(6) N(2)			C(9),C(11)
Pyridine	Py	0.023	C(4),C(68)
N(1) C(2) C(3) C(4) C(5) C(68)			
Benzimidazole 2	Bz2	0.007	N(5)
C(15) C(16) C(17) C(18) C(19) C(20) N(4) C(14) N(5)			
Phenyl	Phen	0.016	C(24)
C(22) C(23) C(24) C(25) C(26) C(27)			
Indolium 1	Ind1	0.036	C(37)
C(36) C(37) C(40) C(41) C(42) C(43) C(44) C(45) N(6)			
Indolium 2	Ind2	0.034	N(7)
C(51) C(52) C(55) C(56) C(57) C(58) C(59) C(60) N(7)			

Interplanar angles (°)

	Bz1	Py	Bz2	Phen	Ind1	Ind2
Bz1		40.14(8)	48.17(7)	47.47(7)	75.53(7)	49.03(9)
Py			8.03(7)	55.64(9)	65.20(8)	86.25(9)
Bz2				59.82(8)	57.45(7)	86.27(8)
Phen					87.16(7)	81.6(1)
Ind1						29.30(8)
Ind2						
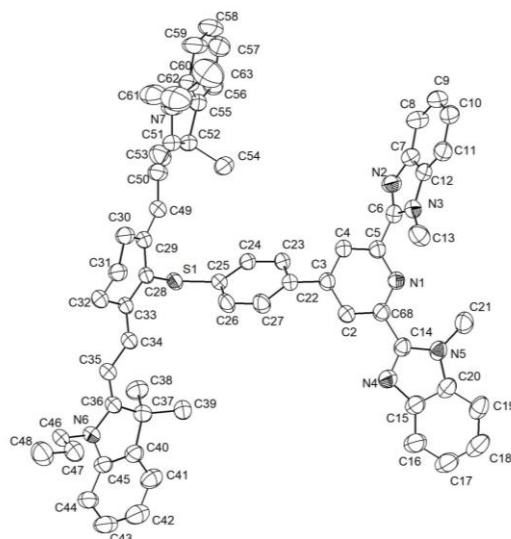
Figure S1. ORTEP molecular view with numbering scheme of the asymmetric unit of [**L6**]$^+$ in the crystal structure of [**L6**](PF$_6$). Thermal ellipsoids are represented at 50% probability level and hydrogen atoms, PF$_6^-$ counterion and disordered solvate molecules (Et$_2$O and CH$_2$Cl$_2$) are omitted for clarity.

Table S4. Summary of crystal data, intensity measurements and structure refinements for complex [**L6**Er(hfa)$_2$(O$_2$CCF$_3$)](PF$_6$)·(CH$_3$CH$_2$)$_2$O.

	[**L6**Er(hfa)$_2$(O$_2$CCF$_3$)](PF$_6$)·(CH$_3$CH$_2$)$_2$O
Empirical formula	C$_{79}$H$_{76}$ErF$_{21}$N$_7$O$_7$PS
Chemical formula moiety	C$_{75}$H$_{66}$ErF$_{15}$N$_7$O$_6$S, F$_6$P, C$_4$H$_{10}$O
Formula weight	1864.75
Temperature	120.00(13) K
Wavelength	1.54184 Å
Crystal System, Space group	Triclinic, P -1
Unit cell dimensions	a = 9.36238(12) Å, b = 21.3267(3) Å, c = 21.74321(19) Å, α = 111.9800(10)°, β = 96.2788(9)°, γ = 93.9101(11)°
Volume in Å^3	3973.58(9)
Z, Calculated density	2, 1.559 Mg/m^3
Absorption coefficient	3.347 mm^{-1}
F(000)	1886
Theta range for data collection	2.215 to 67.405°
Limiting indices	-11≤h≤11, -25≤k≤25, -22≤l≤26
Reflections collected / unique	93868 / 14176 [R(int) = 0.0359]
Completeness to theta	67.406°/ 99.1 %
Data / restraints / parameters	14176 / 6 / 1086
Goodness-of-fit on F^2	1.060
Final R indices [I>2σ(I)]	R_1 = 0.0792, ωR_2 = 0.2060
R indices (all data)	R_1 = 0.0879, ωR_2 = 0.2125
Largest diff. peak and hole	1.492 and -1.216 e.Å^{-3}

Table S5. Selected bond distances (Å) and bond angles (°) for complex [**L6**Er(hfa)$_2$(O$_2$CCF$_3$)](PF$_6$)·(CH$_3$CH$_2$)$_2$O.

Bond distances (Å)

Atom 1	Atom 2	Distance	Atom 1	Atom 2	Distance
Er(1)	O(1)	2.367(5)	Er(1)	N(1)	2.512(5)
Er(1)	O(2)	2.314(5)	Er(1)	N(2)	2.428(5)
Er(1)	O(3)	2.288(4)	Er(1)	N(4)	2.459(5)
Er(1)	O(4)	2.319(5)	S(1)	C(25)	1.765(6)
Er(1)	O(5)	2.687(8)	S(1)	C(28)	1.793(6)
Er(1)	O(6)	2.415(7)			

Angles (°)

At. 1	At. 2	At. 3	angle	At. 1	At. 2	At. 3	angle
O(1)	Er(1)	O(5)	131.5(2)	O(3)	Er(1)	N(4)	78.87(17)
O(1)	Er(1)	O(6)	135.31(19)	O(4)	Er(1)	O(1)	68.9(2)
O(1)	Er(1)	N(1)	121.08(16)	O(4)	Er(1)	O(5)	66.9(2)
O(1)	Er(1)	N(2)	74.23(16)	O(4)	Er(1)	O(6)	76.8(2)
O(1)	Er(1)	N(4)	139.89(17)	O(4)	Er(1)	N(1)	145.15(19)
O(2)	Er(1)	O(1)	72.04(17)	O(4)	Er(1)	N(2)	88.69(18)
O(2)	Er(1)	O(4)	137.64(19)	O(4)	Er(1)	N(4)	131.92(19)
O(2)	Er(1)	O(5)	137.2(2)	O(6)	Er(1)	O(5)	47.9(2)
O(2)	Er(1)	O(6)	145.2(2)	O(6)	Er(1)	N(1)	74.9(2)
O(2)	Er(1)	N(1)	71.37(15)	O(6)	Er(1)	N(2)	77.3(2)
O(2)	Er(1)	N(2)	95.94(17)	O(6)	Er(1)	N(4)	84.61(19)
O(2)	Er(1)	N(4)	73.73(16)	N(1)	Er(1)	O(5)	106.6(2)
O(3)	Er(1)	O(1)	74.52(17)	N(2)	Er(1)	O(5)	122.8(2)
O(3)	Er(1)	O(2)	78.71(17)	N(2)	Er(1)	N(1)	65.56(15)
O(3)	Er(1)	O(4)	75.8(2)	N(2)	Er(1)	N(4)	129.94(16)
O(3)	Er(1)	O(5)	76.4(2)	N(4)	Er(1)	O(5)	67.7(2)
O(3)	Er(1)	O(6)	123.9(2)	N(4)	Er(1)	N(1)	64.74(15)
O(3)	Er(1)	N(1)	137.78(17)	C(25)	S(1)	C(28)	105.5(3)
O(3)	Er(1)	N(2)	148.42(17)				

Table S6. Selected least-squares planes data for complex [**L6**Er(hfa)$_2$(O$_2$CCF$_3$)](PF$_6$)·(CH$_3$CH$_2$)$_2$O.

Least-squares planes

Least-squares planes description	Abbreviation	Max. dev./Å	Atom
Benzimidazole 1 C(7) C(8) C(9) C(10) C(11) C(12) N(4) C(6) N(5)	Bz1	0.014	C(6)
Pyridine N(1) C(1) C(2) C(3) C(4) C(5)	Py	0.006	C(1),N(1)
Benzimidazole 2 C(15) C(16) C(17) C(18) C(19) C(20) N(2) C(14) N(3)	Bz2	0.026	N(3)
Phenyl C(22) C(23) C(24) C(25) C(26) C(27)	Phen	0.020	C(25)
Indolium 1 C(36) C(37) C(40) C(41) C(42) C(43) C(44) C(45) N(6)	Ind1	0.042	C(36)
Indolium 2 C(51) C(52) C(55) C(56) C(57) C(58) C(59) C(60) N(7)	Ind2	0.022	C(55)

Interplanar angles (°)

	Bz1	Py	Bz2	Phen	Ind1	Ind2
Bz1		8.1(2)	15.2(2)	36.1(2)	44.4(2)	54.2(2)
Py			7.6(2)	37.2(2)	36.4(2)	46.8(2)
Bz2				42.7(2)	29.4(2)	39.2(2)
Phen					59.4(2)	74.0(2)
Ind1						14.8(2)
Ind2						
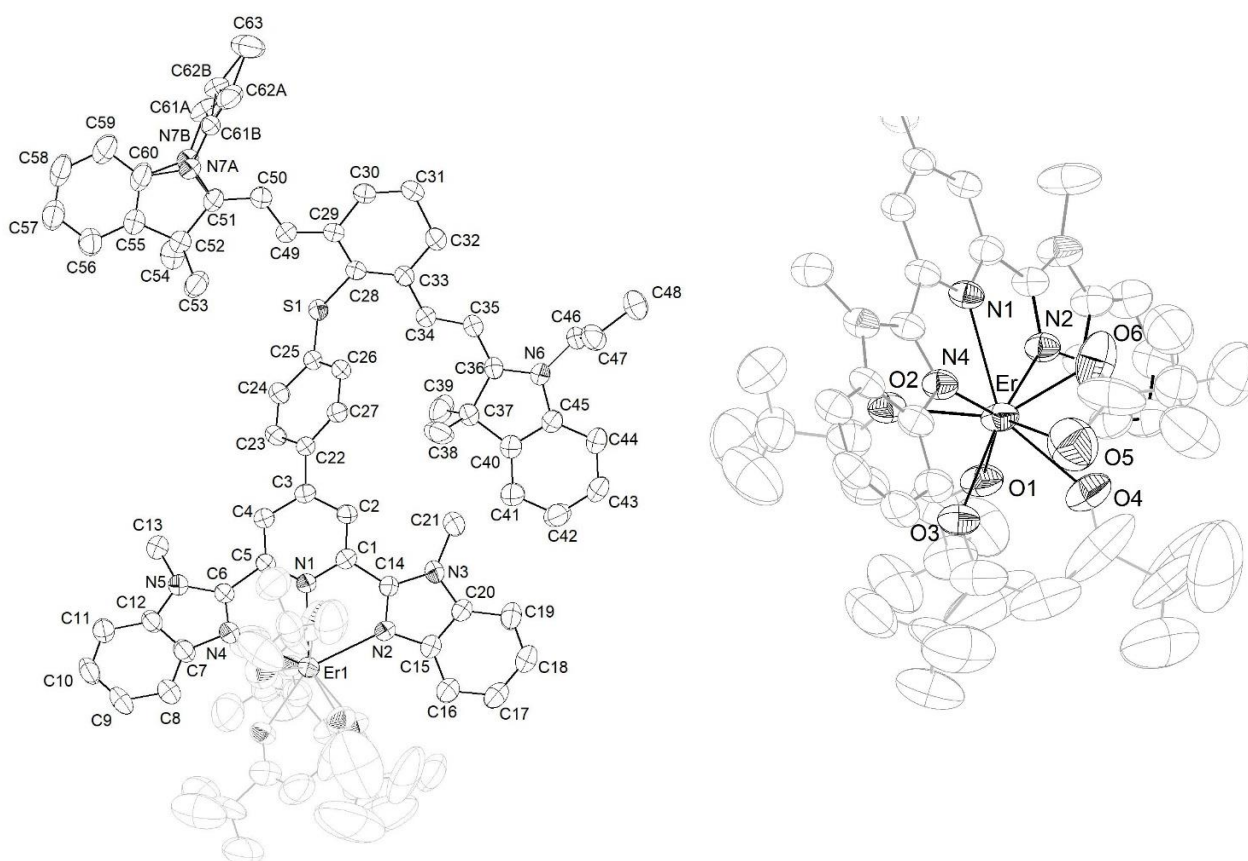
Figure S2. ORTEP molecular view with numbering scheme of the asymmetric unit of [**L6**Er(hfa)$_2$(O$_2$CCF$_3$)]$^+$ in the crystal structure of [**L6**Er(hfa)$_2$(O$_2$CCF$_3$)](PF$_6$)·(CH$_3$CH$_2$)$_2$O. Thermal ellipsoids are represented at 50% probability level and hydrogen atoms, PF$_6$ counter-ion and Et$_2$O solvate molecules are omitted for clarity.

a)

b)
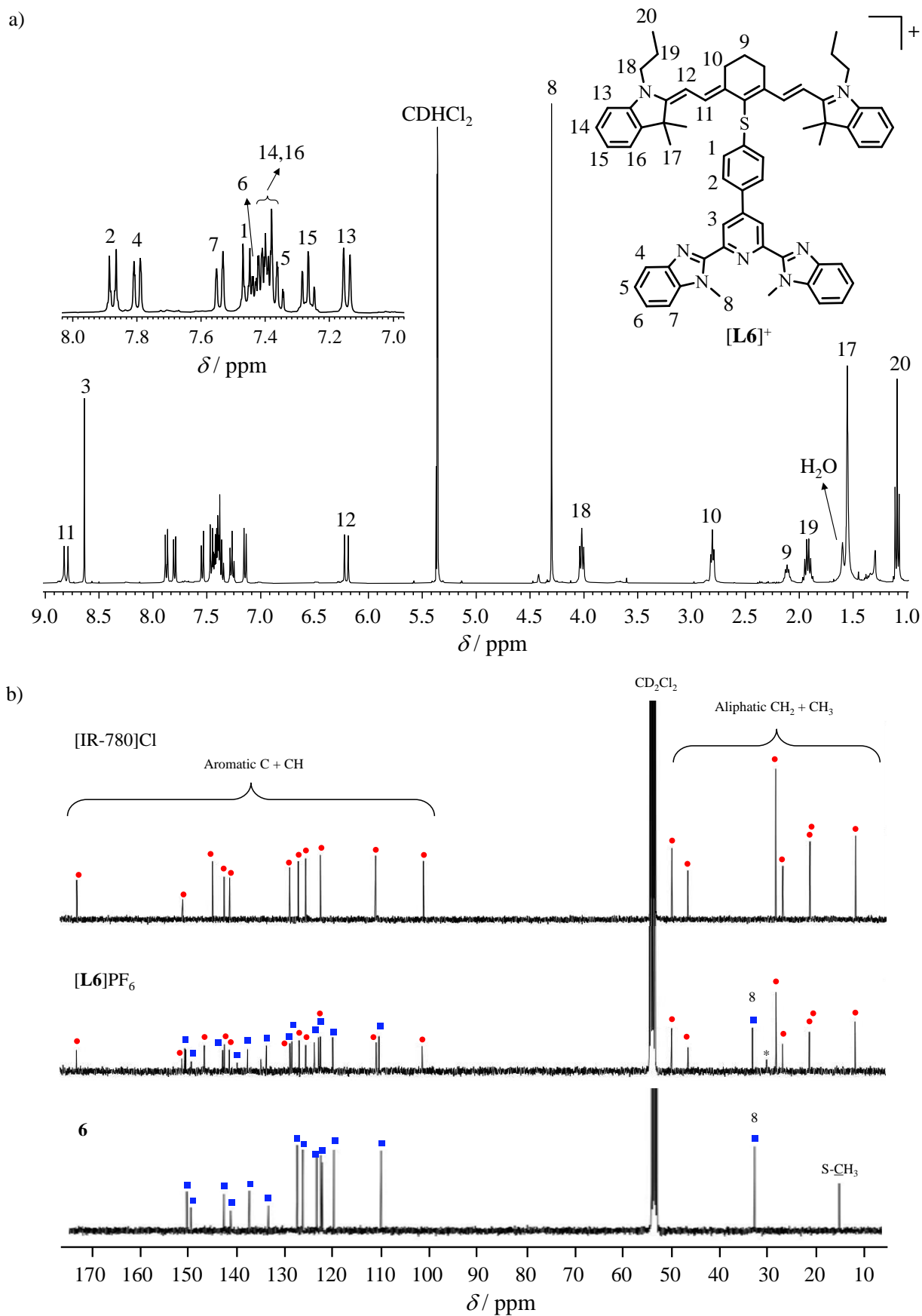
Figure S3. a) ^{1}H NMR spectrum of ligand [**L6**]PF$_6$ and b) ^{13}C NMR spectra of **6**, [IR-780]Cl and [**L6**]PF$_6$ (* = trace of acetone) in CD$_2$Cl$_2$ at 293 K. red points = cyanine dye, blue squares = tridentate binding unit
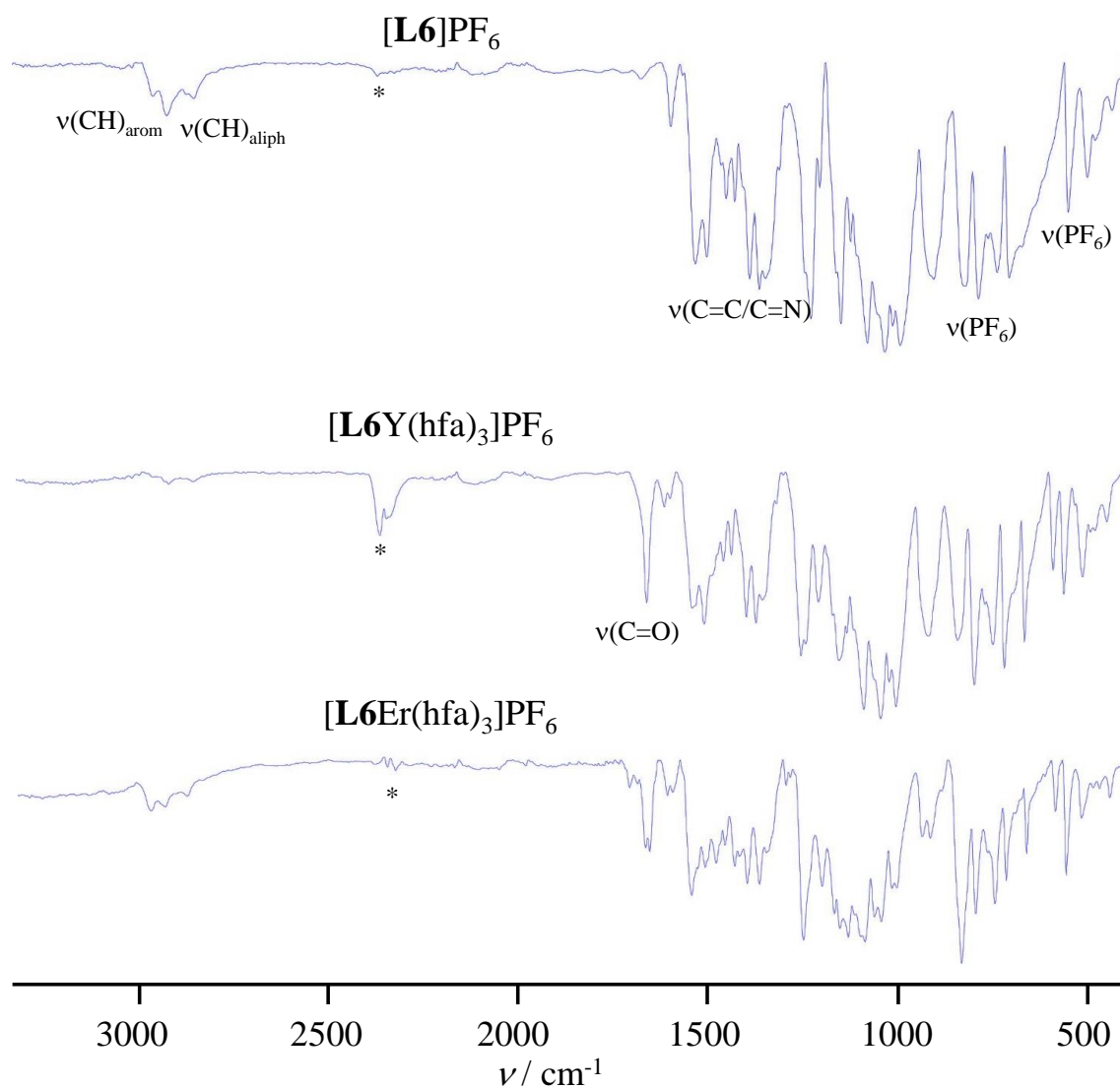
Figure S3c Infra-red spectra of [**L6**]PF$_6$, [**L6**Y(hfa)$_3$]PF$_6$ and [**L6**Er(hfa)$_3$]PF$_6$ (* non-compensated signals for traces of CO_2).
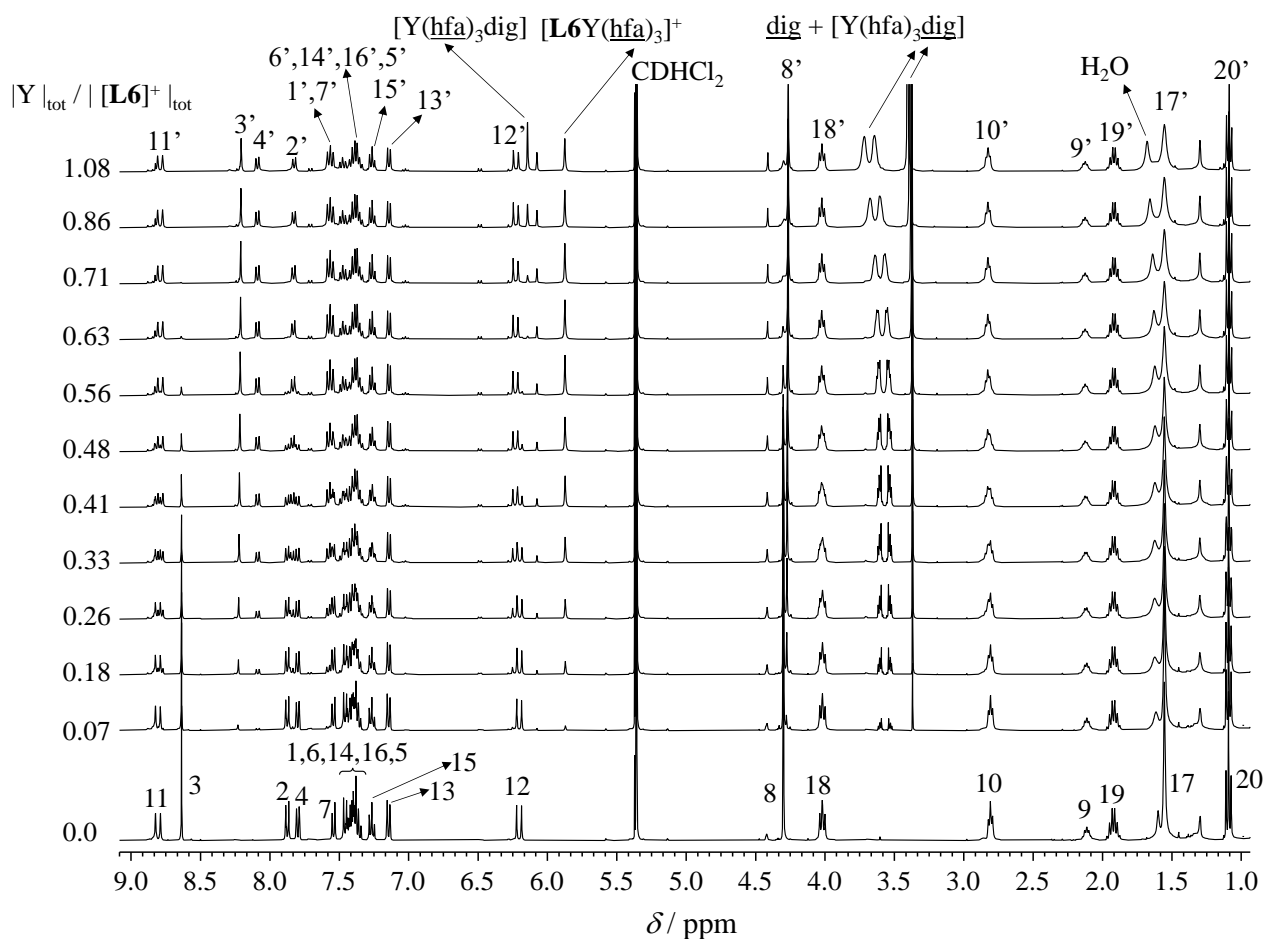
Figure S4. ^{1}H NMR spectra recorded upon titration of [**L6**](PF$_6$) with [Y(hfa)$_3$dig] in CD$_2$Cl$_2$ at 293 K ($5 \cdot 10^{-3} \leq |[\textbf{L6}]^+|_{tot} \leq 6 \cdot 10^{-3}$ M and $4 \cdot 10^{-4} \leq |Y|_{tot} \leq 5 \cdot 10^{-3}$ M; numbering scheme for the protons of the ligand **L6** is given in Figure 2. Numbers with prime (') symbol correspond to the signals arising upon formation of [**L6**Y(hfa)$_3$]$^+$ complex. The signal for hfa co-ligands depend of anion transfer and ion pair formation and are not highlighted.[20,23]
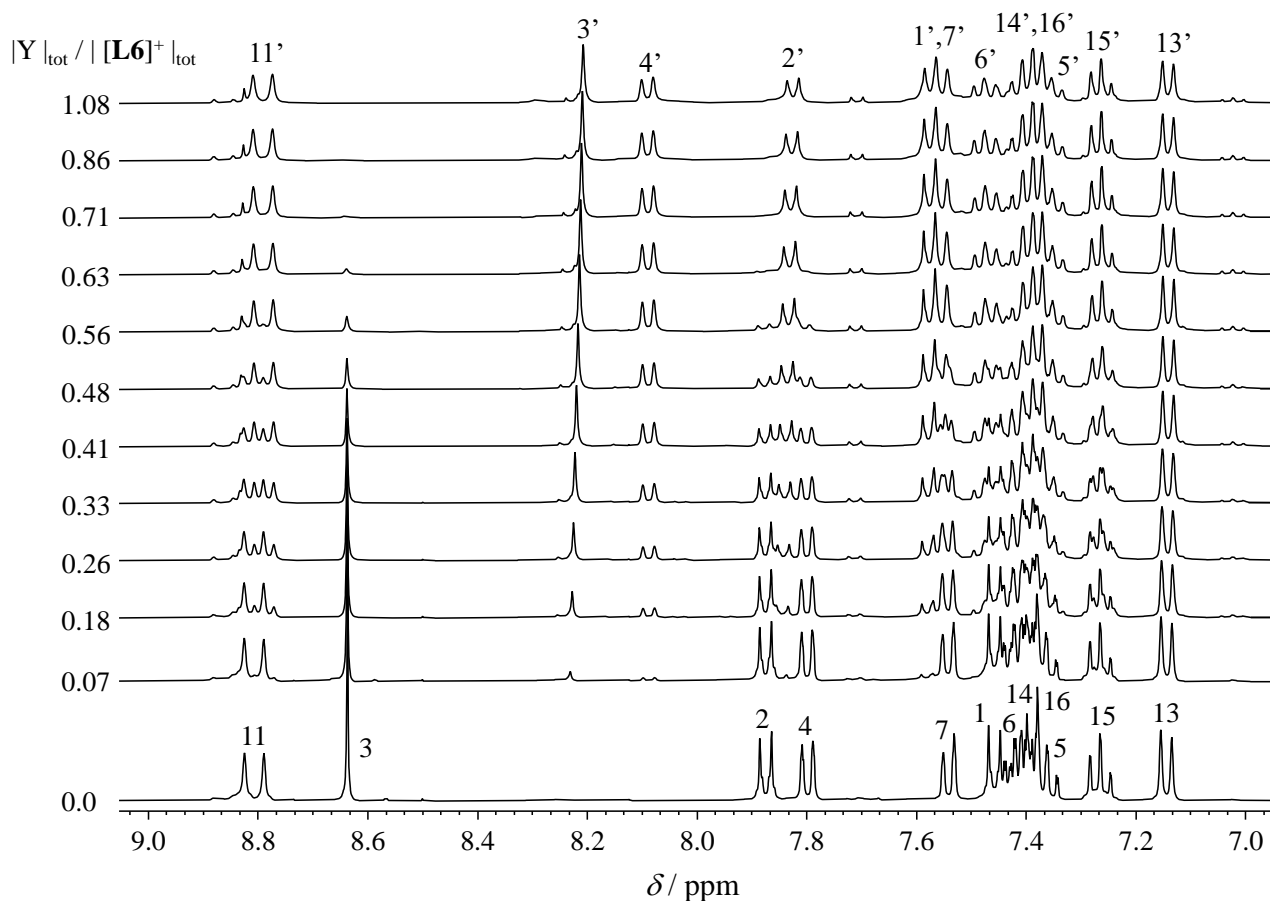
Figure S5. Aromatic parts of the ^{1}H NMR spectra recorded upon titration of [**L6**](PF$_6$) with [Y(hfa)$_3$dig] in CD$_2$Cl$_2$ at 293 K ($5\cdot10^{-3} \leq$ |[**L6**]$^+$|$_{tot} \leq 6\cdot10^{-3}$ M and $4\cdot10^{-4} \leq$ |Y|$_{tot} \leq 5\cdot10^{-3}$ M). The numbering is taken from Figure 2. Numbers with prime (') symbol correspond to the signals arising upon formation of [**L6**Y(hfa)$_3$]$^+$ complex.
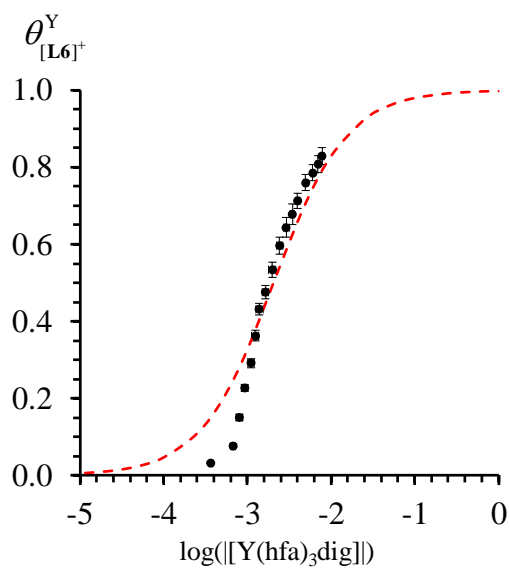
Figure S6.   Experimental (circles) and fitted (dashed red traces using eqn 3) binding isotherm for the titration of [**L6**](PF$_6$) with [Y(hfa)$_3$dig] in CD$_2$Cl$_2$ + 0.14 M diglyme at 293 K ($5 \cdot 10^{-3} \leq |[\mathbf{L6}]^+|_{tot} \leq 3 \cdot 10^{-3}$ M and $5 \cdot 10^{-4} \leq |Y|_{tot} \leq 1 \cdot 10^{-2}$ M).
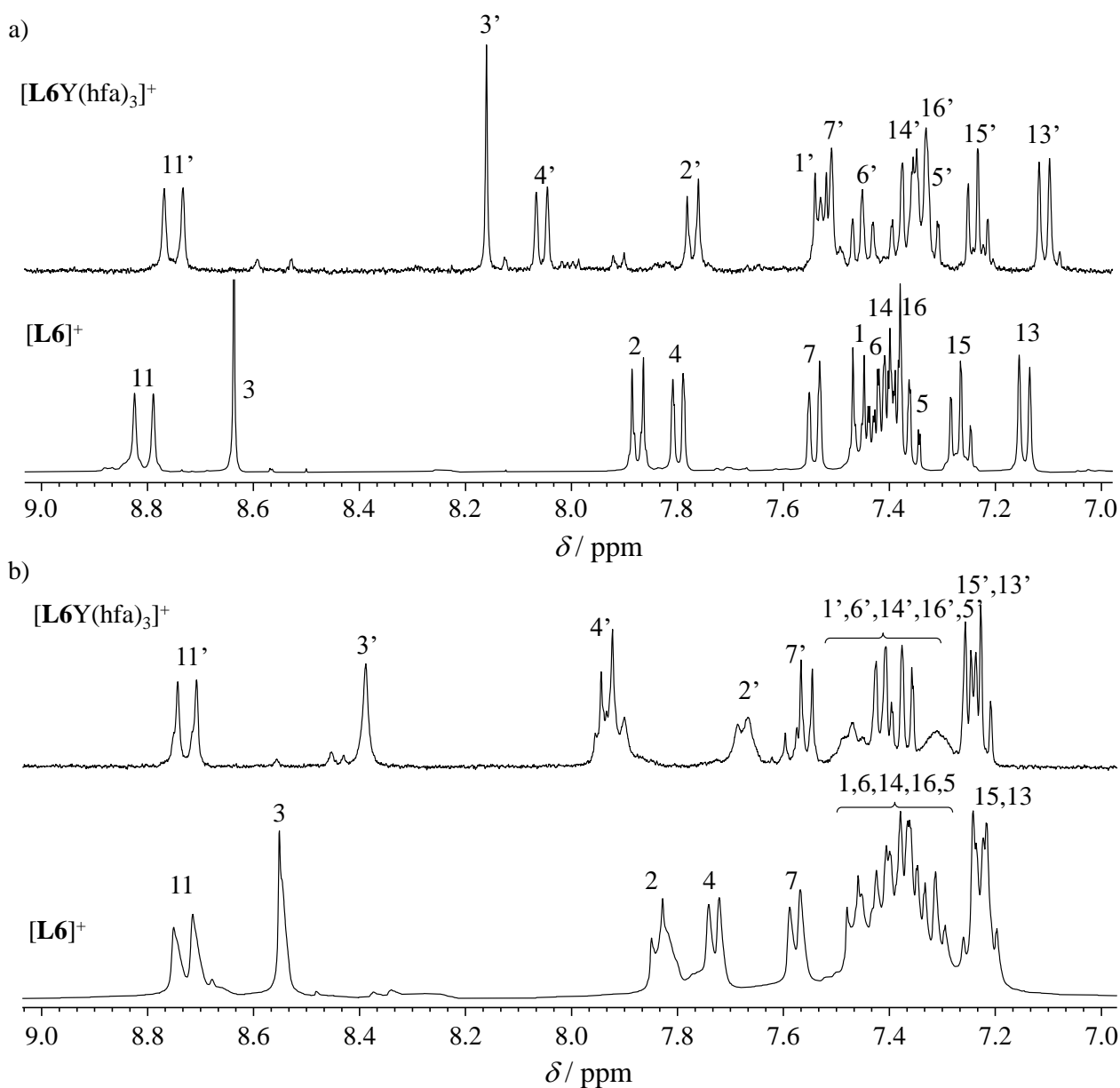
Figure S7. Aromatic parts of the ^{1}H NMR spectra recorded for the ligand [**L6**](PF$_6$) (1·10^{-2} M) and for the [**L6**Y(hfa)$_3$]$^+$ complex (5·10^{-4} M) in a) CD$_2$Cl$_2$ and b) CD$_3$CN at 293 K. The numbering is taken from Figure 2. Numbers with prime (') symbol correspond to the signals of [**L6**Y(hfa)$_3$]$^+$ complex.
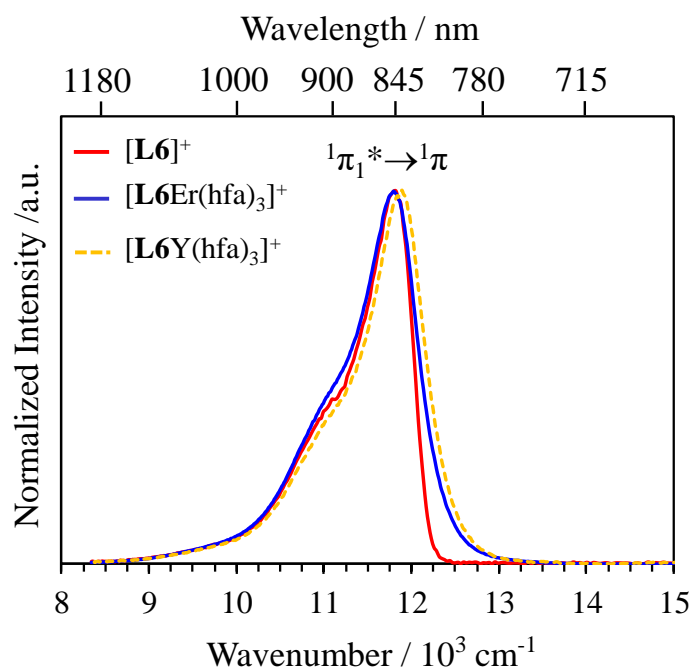
Figure S8. Emission spectra of ligand $[\mathbf{L6}]^+$ (λ_{exc} = 640 nm, $\tilde{v}_{exc}$ = 15625 cm^{-1}) and of $[\mathbf{L6}Ln(hfa)_3]^+$ (Ln = Er and Y) complexes (λ_{exc} = 610 nm, $\tilde{v}_{exc}$ = 16393 cm^{-1}) in acetonitrile solution ($|[\mathbf{L6}]^+|$ = 3·10^{-5} M and $|[\mathbf{L6}Ln(hfa)_3]^+|$ = 5·10^{-4} M) at 293 K. The energies of the peaks are given in the main text.
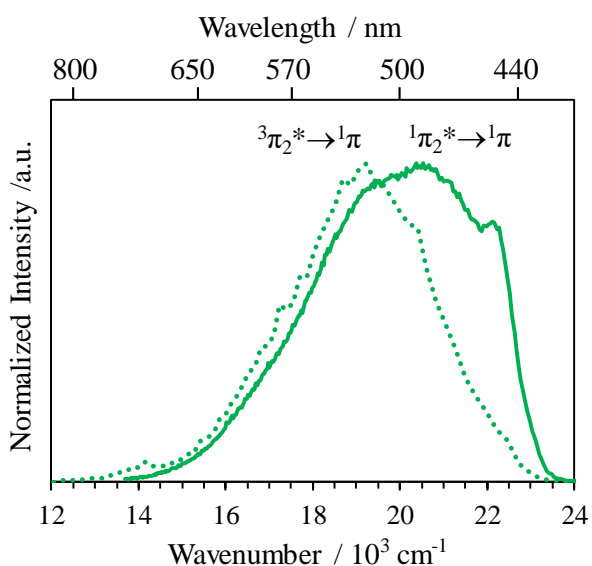
Figure S9. Normalized luminescence (λ_{exc} = 370 nm, $\tilde{v}_{exc}$ = 27027 cm^{-1}, full trace) and time-gated phosphorescence (λ_{exc} = 320 nm, $\tilde{v}_{exc}$ = 31250 cm^{-1}, 100 µs delay, dotted trace) spectra recorded for $[\mathbf{L6}Gd(hfa)_3]^+$ in frozen acetonitrile solution (5·10^{-4} M) at 10 K highlighting the emissions originating from the ligand-centered singlet and triplet states, respectively. The energies of the peaks are given in the main text.
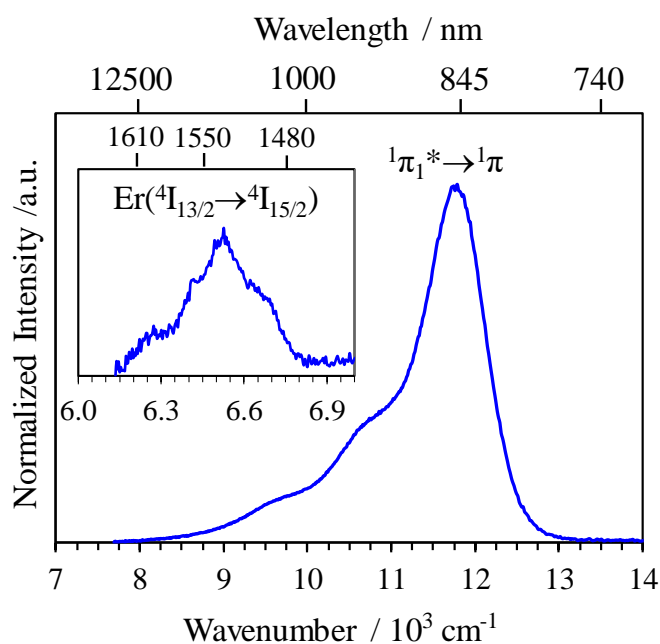
Figure S10. Ligand-centered (main plot) and Er(III)-centered (inset) near-infrared emission spectra recorded for [**L6**Er(hfa)$_3$](PF$_6$) (λ_{exc} = 370 nm, $\tilde{v}_{exc}$ = 27027 cm^{-1}) in the solid state at 298 K. The energies of the peaks are given in the main text.
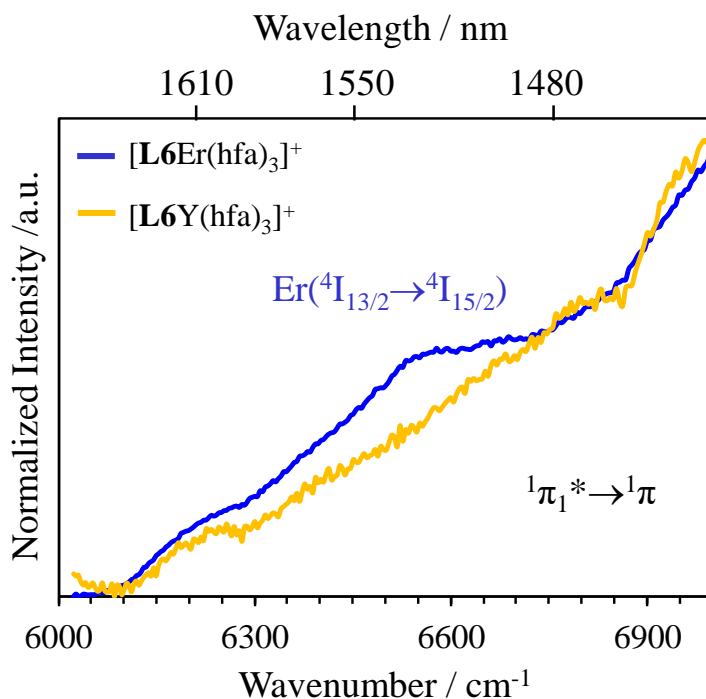
Figure S11. Near-infrared part of the luminescence spectra of [**L6**Ln(hfa)$_3$]$^+$ complexes (Ln = Er and Y) recorded in acetonitrile solution (5·10^{-4} M, 293 K) upon laser excitation at λ_{exc} = 801 nm ($\tilde{v}_{exc}$ = 12284 cm^{-1}, 2.3-5.7 W·cm^{-2}). The energies of the peaks are given in the main text.
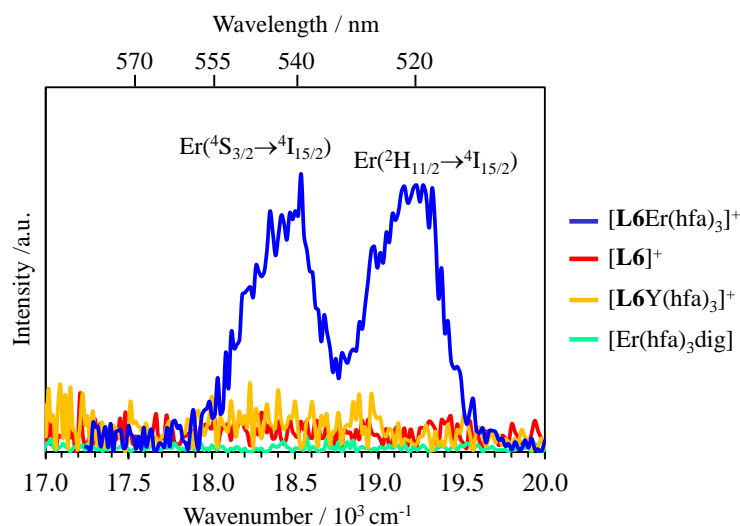
Figure S12. Emission spectra recorded upon NIR laser excitation ($\lambda_{exc} = 801$ nm, $\tilde{\nu}_{exc} = 12284$ cm^{-1}) of [**L6**Er(hfa)$_3$]$^+$ (1.4 W·cm^{-2}), [**L6**]$^+$ (5.1 W·cm^{-2}), [**L6**Y(hfa)$_3$]$^+$ (5.1 W·cm^{-2}) and [Er(hfa)$_3$dig] (5.1 W·cm^{-2}) in acetonitrile solution (5·10^{-4} M) at 293 K. These results highlight the absence of any upconverted signal in the specra recorded for [**L6**]$^+$, [**L6**Y(hfa)$_3$]$^+$ and [Er(hfa)$_3$dig] upon NIR laser excitation. The energies of the peaks are given in the main text.
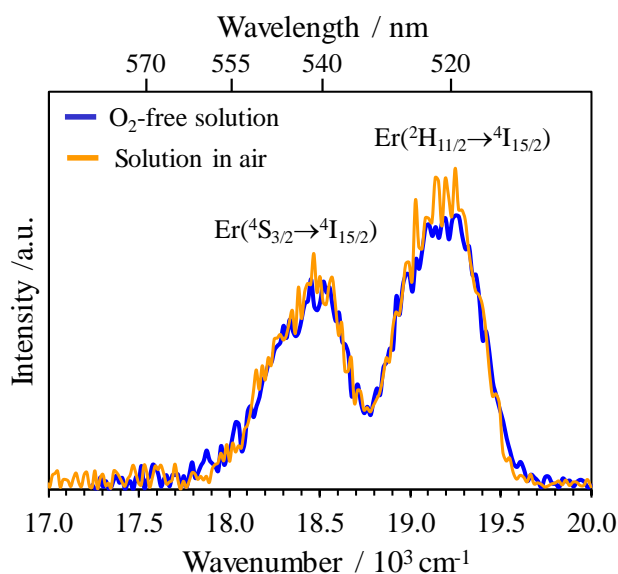
Figure S13. Upconverted visible Er(^{2}H$_{11/2} \rightarrow ^4$I$_{15/2}$) and Er(^{4}S$_{3/2} \rightarrow ^4$I$_{15/2}$) emissions observed for [**L6**Er(hfa)$_3$]$^+$ recorded in acetonitrile solution (5·10^{-4} M, 293 K) upon laser excitation at $\lambda_{exc} = 801$ nm ($\tilde{\nu}_{exc} = 12284$ cm^{-1}, 5.1 W·cm^{-2}). The oxygen-free spectrum (blue) was recorded from the solution which was prepared under an inert atmosphere using degassed solvent. The latter solution was then exposed to air for 24 h at room temperature from which the second spectrum (orange) was recorded using the same laser intensity (5.1 W·cm^{-2}). The energies of the peaks are given in the main text

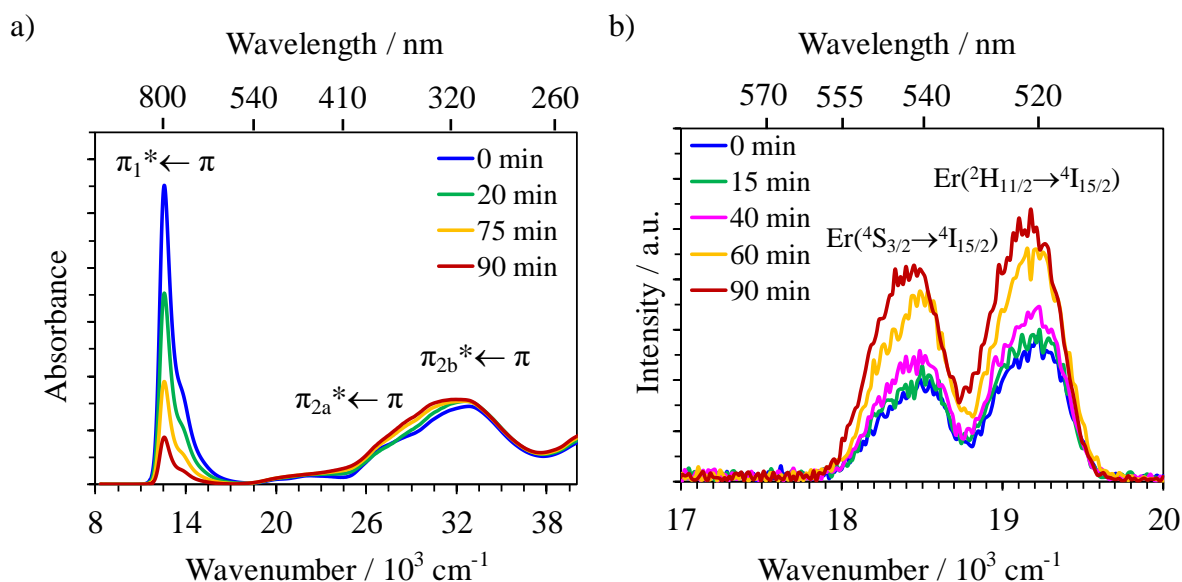**Figure S14**. Monitoring the intensity of a) absorption and b) upconverted emission signals recorded for [**L6**Er(hfa)$_3$]$^+$ in acetonitrile solution (5·10^{-4} M, 293 K) upon continuous laser excitation at $\lambda_{\text{exc}} =$ 801 nm ($\tilde{\nu}_{\text{exc}}$ = 12284 cm^{-1}, 5.7 W·cm^{-2}) over a period of time.
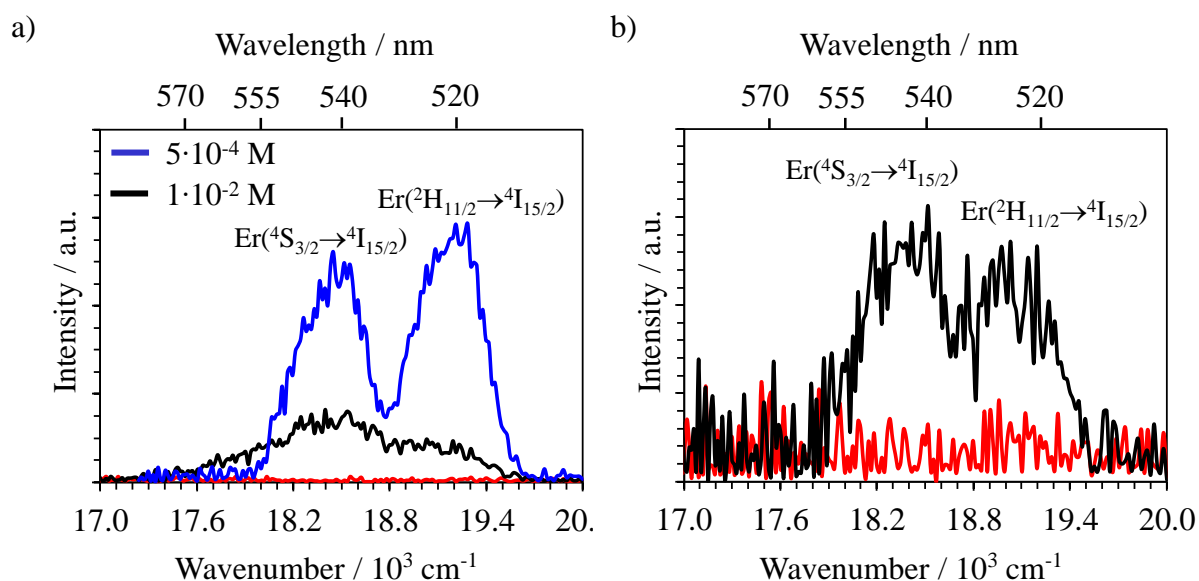
Figure S15. Upconverted visible Er(^{2}H$_{11/2}$→^{4}I$_{15/2}$) and Er(^{4}S$_{3/2}$→^{4}I$_{15/2}$) emissions upon laser excitation at λ_{exc} = 801 nm ($\tilde{\nu}_{\text{exc}}$ = 12284 cm^{-1}) recorded for [**L6**Er(hfa)$_3$]$^+$ a) in acetonitrile solution at two different concentrations (2.5-2.7 W·cm^{-2}) and b) in the solid state (0.6 W·cm^{-2}) at 293 K. The blanks (red curves) were recorded upon irradiation of the pure acetonitrile (for solution, at P = 5.1 W·cm^{-2}) or the copper plate support covered with silver glue (for the solid state, at P = 0.6 W·cm^{-2}).